THE JOURNAL OF PHYSICAL CHEMISTRY B

Article

pubs.acs.org/JPCB

Phase Diagram of Diblock Copolymers Confined in Thin Films

Weihua Li,* Meijiao Liu, and Feng Qiu

State Key Laboratory of Molecular Engineering of Polymers, Department of Macromolecular Science, Fudan University, Shanghai 200433, China

An-Chang Shi*

Department of Physics and Astronomy, McMaster University, Hamilton, Ontario, Canada, L8S 4M1

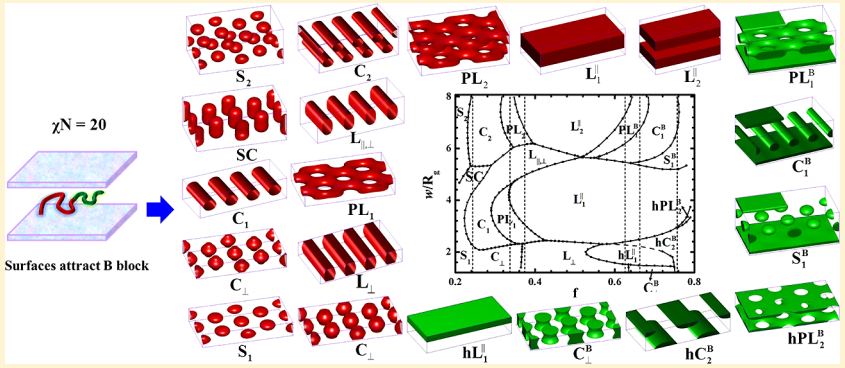

ABSTRACT: The phase behaviors of diblock copolymers confined in thin films with two identical preferential surfaces are investigated using the self-consistent field theory. Around 20 morphologies, including centrosymmetric and non-centrosymmetric ones, are considered to construct the two-dimensional phase diagram with respect to the volume fraction and the film thickness, while the interaction parameter χN and the surface preferences are fixed. When these morphologies are classified into four categories of ordered phases—sphere, cylinder, perforated lamella (corresponding to gyroid phase in bulk), and lamella—the phase diagram directly reveals the impact of the film confinement on the order−order transitions as a function of volume fraction via the comparisons to those in bulk. Our results also provide a comprehensive understanding over the dependence of the structure formations on the film thickness for each volume fraction.

I. INTRODUCTION

The self-assembly of block copolymers (BCPs) has attracted great attention because it provides a platform to fabricate a large number of ordered nanostructures which not only have wide potential applications in the manufacture of nanoscale functional materials but also have rich fundamental statistical physics. Particularly, the fast development of the nanolithography technique based on the BCP self-assembly to make large-scale ordered patterns, which extends the feature size of the nanostructures obtained by the e-beam or extreme ultraviolet lithography further into smaller size (sub-30-nm), pushes the application of BCP self-assembly further toward real implementation.[1−8] In experiments, usually the BCPs are spin-coated onto a substrate to form film in either thermal annealing or solvent annealing treatment to investigate their self-assembling behaviors. Both the bottom surface of the substrate and the top surface formed by the interface of air or other solvent vapor have significant influences on the formation of structures, especially in the case of thin film. For example, symmetric diblock copolymer prefers to form perpendicular lamellae for neutral surfaces, while to form layers parallel with the film surfaces or even mixed morphologies for preferential surfaces in thin films.[9−29]

The BCP self-assembly in thin films has been extensively studied to understand the different phase behaviors from those in bulk, induced by the factors arising from the presence of the two surfaces, i.e., the energetic preferences of surfaces for one of the two blocks and the geometrical confinement, by both experiments[9−13,30−39] and theories.[14−29,40−52] For lamella-forming symmetric diblock copolymers (DBCs), most of the experiments have been dedicated to control the lamella orientation by tuning the film thickness and the interactions between the surfaces and the blocks. Furthermore, a number of experiments have observed some complex or unconventional morphologies in thin films formed by the supporting substrate and a top air/copolymer interface (see the summary in ref 29). In ref 29, Meng and Wang have carried a systematical self-consistent field theory (SCFT) study to explore the phase behaviors of symmetric DBCs confined in thin films. For example, they observed complex morphologies of T_k (k = 1, 2, 3) for asymmetric surface interactions, which are composed of k layers of regular lamellae

Received: September 26, 2012
Revised: February 23, 2013
Published: April 2, 2013

   dx.doi.org/10.1021/jp309546q | J. Phys. Chem. B 2013, 117, 5280−5288

and a single layer of perforated lamella. When symmetric DBCs are replaced by asymmetric DBCs, more complicated phase behaviors are expected. Therefore, more and more research efforts tend to be concentrated on the system of asymmetric DBCs in thin films.[31−50] Wang et al. have given a summary on the experimental observations of the cylindrical bulk morphology confined in thin films.[43] In these experiments,[30,32−37] a variety of morphologies, including cylindrical (parallel/perpendicular cylinders or parallel half-cylinders) and noncylindrical morphologies (spheres, lamellae, or parallel perforated lamellae), have been observed with various film thicknesses and surface preferences. In a series of experimental and theoretical studies,[53−55] Kramer and co-workers have systematically investigated the packing transition of spheres in films as a function of the film thickness. Their results exhibit that the 2D spheres packing is hexagonal when the layers are less than 4, and then it transfers to orthorhombic for more layers. As the layer number is further increased from 5 to 23, the orthorhombic unit cell deforms continuously to that of the body cubic-centered (110) one. In a word, the presence of the top/bottom surfaces not only influences the domain orientation but also strongly influences the phase itself, i.e., the order−order transition (OOT).[51]

In theory, a usual and easy way is to model BCP thin films as BCPs under the confinement of two impenetrable surfaces on which appropriate surface potentials are imposed according to surface properties. An obvious approximation that the top surface between the BCPs and the air is simplified as a rigid surface has been introduced into this model. In real BCP film, the top surface is free and can have fluctuation because of the formation of heterogeneous structures as well as the thermal fluctuation. Though there are some discrepancies between this theoretical model with the real BCP films in experiments, it still attracts a lot of theoretical research attention because of its two main features. One is that the BCP phase behaviors can be enriched dramatically in the simplest geometrical confinement (one-dimensional, 1D) by tuning the film thickness, the surface preferential interactions, and the parameters of BCP itself. The second is that the knowledge of the BCP phase behaviors in this model system can provide a qualitative understanding on the experimental observations in BCP film systems.

Even for the simple DBC system, besides the volume fraction of the A block, $f = f_A$, and the interaction parameter which is the product χN of the Flory−Huggins interaction, χ, and the total degree of polymerization, N, there are still a number of factors affecting the phase behaviors, including the film thickness and the preferences of the two surfaces to different blocks (symmetric or asymmetric surface interactions). In past decades, most of theoretical work on asymmetric DBCs in thin films, including computer simulations[40−45] and SCFT calculations,[46−49] focus on the effects of the film thickness and the surface interactions including their preference and strength for a typical volume fraction of symmetric or asymmetric DBC. Huinink et al.[40,41] employed a dynamic density functional theory (DDFT or dynamic SCFT), to simulate the self-assembling behavior of DBCs with $f = 1/3$ confined between two identical surfaces. They systematically explored the formation of morphologies including parallel/perpendicular cylinders, parallel lamellae, and perforated lamellae (PL) with various film thicknesses and surface interaction strengths from negative (A-preferential), to zero (neutral), to positive (B-preferential). In a subsequent work,[42,56] Sevink and co-workers studied the structure formation of sphere-forming AB diblock and ABA triblock copolymers with $f = 1/3$ confined in thick films with varying film thickness and surface potential. A thin film system of asymmetric DBCs, with a smaller volume fraction of $f = 1/4$, was extensively studied using Monte Carlo (MC) simulations by Wang et al.[43] Besides the types of parallel/perpendicular cylinders, they also observed one layer of spheres between two wetting A layers for A-preferential surfaces, blending parallel and perpendicular cylinders for B-preferential surfaces, and parallel cylinders containing top and bottom layers of half-cylinders for neutral surfaces. More recently, Yu et al.[45] have simulated the cylinder-forming DBC films with $f = 1/6$ and $f = 1/4$ using MC simulations. Besides the cylinder-forming DBCs, Yin et al.[28] have carried out a study of MC simulations on the gyroid-forming DBC films. Tan et al.[44] have investigated a sphere-forming DBC with $f = 1/5$ in films using the DDFT simulations. In addition, a few SCFT studies based on SCFT calculations have been reported on the formation of morphologies of asymmetric DBCs with a fixed value of f confined between two surfaces.[46−48] These results will be discussed and compared with our results. Most of these studies have focused on the exploration of new morphologies,[47] or roughly sketching the phase diagram with respect to the film thickness and the strength of surface interactions.[48] These results have qualitatively shown the strong dependence of the OOTs on these factors of the DBC films, i.e., the film thickness and the surface interactions. However, they are not enough to provide a quantitative understanding on these complicated self-assembling behaviors, such as the shift of OOTs compared with those in bulk, and the change of domain spacing induced by the confinement.

Besides the two factors, the volume fraction is also often used to tune the morphology formation. To gain a direct and comprehensive understanding over the impact of the film confinement on the OOTs, we focus on the exploration of the phase diagram with respect to the volume fraction and the film thickness while fixing the interaction parameter χN and the surface preferential interactions. In order to narrow our investigation further, we assume that both surfaces have the same preferential interactions to any block. This assumption is clearly unrealistic for many types of DBC films in real experiments, but it serves as a simple starting point for understanding the self-assembling behaviors of DBCs in thin films. Without loss of generality, we chose the surfaces to have preferential interactions to the B block. This implies that the two surfaces attract the majority block for $f < 0.5$, and otherwise they attract the minority block, when f is varied from zero to 1 to go through the bulk phase sequence from disorder, sphere, cylinder, gyroid, to lamella, and then to go through the reverse sequence of gyroid, cylinder, sphere, and disorder. The phase diagram can provide a direct comparison between the OOTs in thin films with varying film thickness and those in bulk, which shows the dependence of the OOT shifts on the film thickness, relative to the bulk ones. Therefore, it can help one to gain an explicit picture of the phase behaviors of BCPs under the confinement of thin films. In addition, it can become a useful guide for experiments to fabricate different morphologies in BCP thin films, which is the most fundamental and indispensable step to realize the application of BCP self-assembly.

II. THEORY

We consider an incompressible melt of AB diblock copolymers with a degree of polymerization N confined in a thin film with two identical surfaces and thickness of w. The chain lengths of the A and B blocks are specified by fN and $(1 - f)N$, respectively.

dx.doi.org/10.1021/jp309546q | J. Phys. Chem. B 2013, 117, 5280−5288

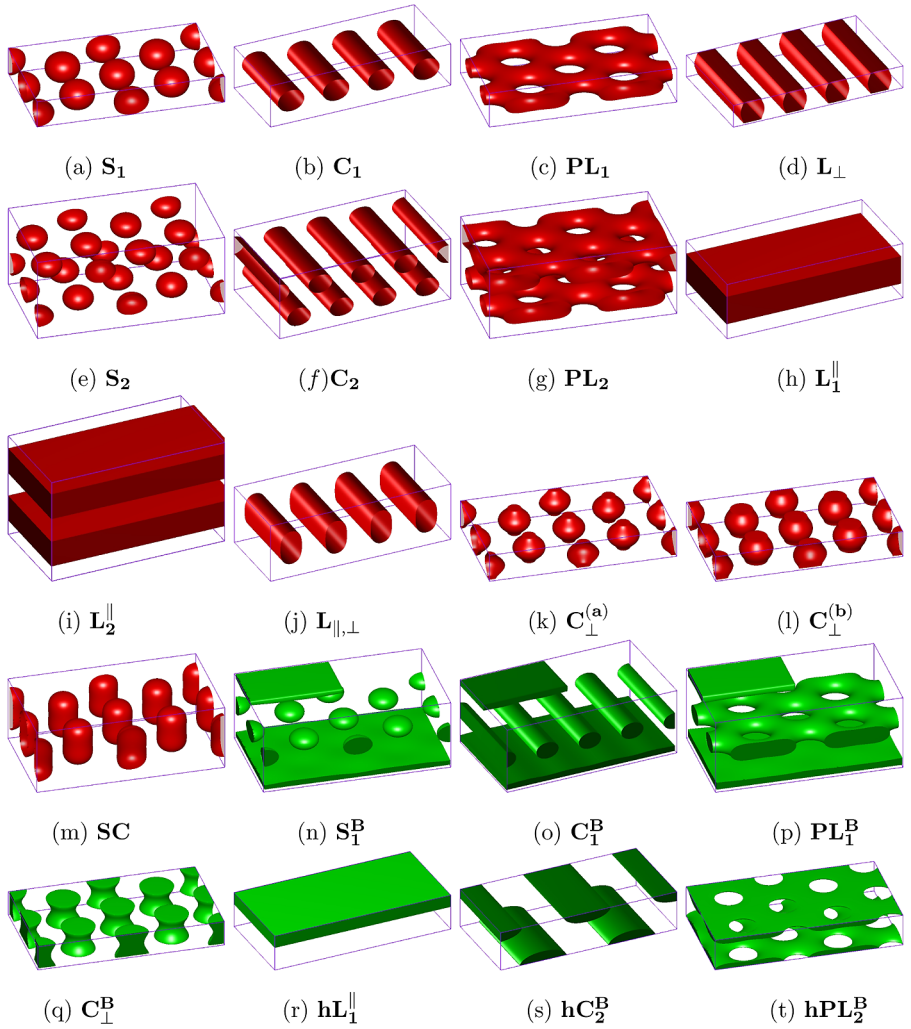

Figure 1. Density isosurface plots of morphologies formed by AB diblock copolymers confined in two identical surfaces with attractive interactions to B block. When the surfaces attract the majority block for $f = f_A < 0.5$, the isosurfaces of the A component are plotted in red color, and otherwise, the isosurfaces of the B component are plotted in green color. Two morphologies of phase $\mathbf{C}_\perp$, with small and large connecting necks with the surfaces, are indicated by $\mathbf{C}_\perp^{(a)}$ and $\mathbf{C}_\perp^{(b)}$, respectively.

The total volume available for polymer chains is V, and the radius of gyration of the polymer, R_g, is set as the unit of spatial lengths in our calculations. Within the mean-field approximation to statistical mechanics of the Edwards model of polymers,[57,58] the free energy functional F for n Gaussian diblock copolymer chains at a given temperature T is given by

$$\frac{F}{nk_BT} = -\ln Q + \frac{1}{V}\int d\mathbf{r}\{\chi N\phi_A(\mathbf{r})\phi_B(\mathbf{r}) - w_A(\mathbf{r})\phi_A(\mathbf{r}) - w_B(\mathbf{r})\phi_B(\mathbf{r}) + H(\mathbf{r})[\phi_A(\mathbf{r}) - \phi_B(\mathbf{r})] - \eta(\mathbf{r})[1 - \phi_A(\mathbf{r}) - \phi_B(\mathbf{r})]\} \quad (1)$$

where $\phi_A(\mathbf{r})$ and $\phi_B(\mathbf{r})$ are the local concentrations of the A and B components, respectively. The quantity Q is the partition function of a single polymer chain interacting with the mean fields w_A and w_B, and which are produced by the surrounding chains. Here the space function $H(\mathbf{r})$, describing the preferential interactions of two identical surfaces on the blocks, is given by

$$\frac{H(\mathbf{r})}{\chi N} = V_0\{\exp[(\sigma - d_z)/\lambda] - 1\} \quad (2)$$

when the distance to surfaces, d_z, is shorter than σ; otherwise, it equals to zero. V_0 and λ quantify the strength and the steepness of the surface interaction, respectively. In this work, we chose $\sigma = 0.5R_g$, $\lambda = 0.25R_g$, and $V_0 = 0.1$, which is equivalent to the interaction strength on the surface in ref 59. $H_s \approx 0.64$, quantifying rather strong surface interactions. Minimization of the free energy with respect to the monomer densities and the mean fields leads to the following SCFT equations[58]

$$w_A(\mathbf{r}) = \chi N\phi_B(\mathbf{r}) + H(\mathbf{r}) + \eta(\mathbf{r})$$
$$w_B(\mathbf{r}) = \chi N\phi_A(\mathbf{r}) - H(\mathbf{r}) + \eta(\mathbf{r})$$
$$\phi_A(\mathbf{r}) = \frac{1}{Q}\int_0^f ds\, q(\mathbf{r}, s)q^\dagger(\mathbf{r}, s)$$
$$\phi_B(\mathbf{r}) = \frac{1}{Q}\int_f^1 ds\, q(\mathbf{r}, s)q^\dagger(\mathbf{r}, s)$$
$$Q = \frac{1}{V}\int d\mathbf{r}\, q(\mathbf{r}, s)q^\dagger(\mathbf{r}, s)$$
$$\phi_A(\mathbf{r}) + \phi_B(\mathbf{r}) = 1 \quad (3)$$

dx.doi.org/10.1021/jp309546q | J. Phys. Chem. B 2013, 117, 5280−5288

In the above equations, $q(\mathbf{r}, s)$ and $q^{\dagger}(\mathbf{r}, s)$ are end-segment distribution functions.[57,58] These distribution functions satisfy the modified diffusion equations

$$\frac{\partial q(\mathbf{r}, s)}{\partial s} = \nabla^2 q(\mathbf{r}, s) - w(\mathbf{r}, s) q(\mathbf{r}, s) \quad (4)$$

$$-\frac{\partial q^{\dagger}(\mathbf{r}, s)}{\partial s} = \nabla^2 q^{\dagger}(\mathbf{r}, s) - w(\mathbf{r}, s) q^{\dagger}(\mathbf{r}, s) \quad (5)$$

where $w(\mathbf{r}, s) = w_A(\mathbf{r})$ when $s < f$, and otherwise $w(\mathbf{r}, s) = w_B(\mathbf{r})$. The initial conditions are $q(\mathbf{r}, 0) = q^{\dagger}(\mathbf{r}, 1) = 1$. For numerical solutions, we employ the pseudospectral method[60,61] to solve the modified diffusion equations for the end-segment distribution functions.

III. RESULTS AND DISCUSSION

We chose the interaction parameter as $\chi N = 20$. We first perform our SCFT calculations, with the space lattice of $N_x \times N_y \times N_z = 64^3$ and the contour discritization of $\Delta s = 0.01$, to identify the OOTs in the bulk. The sphere-to-cylinder, cylinder-to-gyroid, and gyroid-to-lamella OOTs are $f_{S\to C} \approx 0.243$, $f_{C\to G} \approx 0.338$, and $f_{G\to L} \approx 0.374$, respectively, which are in good agreement with those computed using the spectral method by Matsen and Bates.[62] Then, we use two identical rigid walls to geometrically confine the DBC melts in the z direction, and use periodic boundary conditions for the unconfined x and y directions. A rather strong short-range potential as a function of the distance normal to the surfaces in expression 2 with $V_0 = 0.1$ is imposed on the two blocks to act as the preferential interactions. The positive potential strength indicates that the surfaces prefer the B block. For the calculations of centrosymmetric morphologies, the space lattice is chosen as $N_x \times N_y \times N_z = 64^3$, and Δs is always fixed as 0.01. While considering non-centrosymmetric morphologies, we remodel a system with twice the film thickness and an additional wall in the middle of the system according to the scheme proposed by Heckmann and co-worker.[48] Accordingly, twice the space lattice at the z direction, $N_z = 128$, is used. With the knowledge of all possible morphologies found in the previous studies, more than 20 morphologies are produced, and their stabilities are examined by comparing their free energy, for the DBCs confined in thin films of film thickness ranging from $1.2R_g$ to $8R_g$. Nineteen stable morphologies and their phase diagram are presented in Figures 1 and 2, respectively. There are 14 centrosymmetric morphologies, most of which are single-layer morphologies except for the double-layer homogeneous lamellae (denoted as $L_2^{\parallel}$), including A spheres (S_1), parallel A cylinders (C_1, which is denoted as $C_{\parallel}^1$ in ref 48), A perforated lamella (PL_1), perpendicular/parallel A lamellae ($L_{\perp}/L_1^{\parallel}$), perpendicular A cylinder ($C_{\perp}$), z-direction elongated parallel A cylinders ($L_{\parallel,\perp}$)/A spheres (or spherocylinders, SC), B spheres (S_1^B, which is denoted as $L_{\parallel} - S - L_{\parallel}$ in ref 43), B cylinders (C_1^B, which is denoted as $L_{\parallel} - C_{\parallel}^1 - L_{\parallel}$ in ref 43), B perforated lamella (PL_1^B), perpendicular B cylinders ($C_{\perp}^B$), and double B half-perforated layers (hPL_2^B). The other non-centrosymmetric morphologies are one-layer parallel B half lamella ($hL_1^{\parallel}$) and four double-layer morphologies of A spheres (S_2), A cylinders (C_2), A perforated lamellae (PL_2), and B half-cylinders (hC_2^B). For the convenience of free-energy minimization, all of these morphologies have been regulated to align along the sides of the simulation box, i.e., the x and y directions, by special initial conditions. Therefore, we can readily determine the most-favorable domain spacing in the unconfined xy plane by minimizing the free energy, such as the nearest neighbor distance of spheres in spherical morphologies, that of cylinders in cylindrical morphologies, and that of holes in perforated lamellae. Note that the size relation of L_x:$L_y = 2$:$\sqrt{3}$ is employed for the phases with hexagonal symmetry, where the grid spacings at the x and y directions are close.

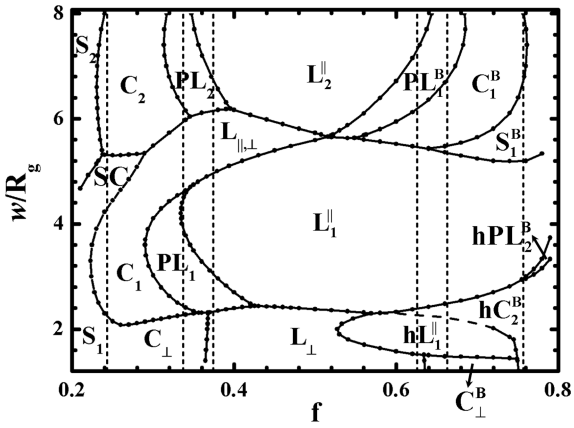

Figure 2. Phase diagram of AB diblock copolymers of fixed $\chi N = 20$ in a thin film with respect to the volume fraction of the A block and the film thickness, w, in units of R_g. Both surfaces have attractive interactions with a strength of $V_0 = 0.1$. The dots are calculated phase transition points, while the curves are guides to the eye, indicating the phase boundaries. The dashed lines indicate the phase transitions between sphere and cylinder, cylinder and gyroid, and gyroid and lamella in the bulk.

In Figure 2, the phase diagram is constructed by more than 200 transition points (the connecting curves are guides to the eye), which are identified by the comparison of free energy between different morphologies. The dashed lines indicate the order−order transitions between sphere and cylinder, cylinder and gyroid, and gyroid and lamella, in the bulk. Although the phase diagram is much more complex than that in the bulk, there are two notable features. In the bulk, the PL phase is not stable, but the gyroid phase is. Therefore, the first feature is that a few PL phases (PL_1, PL_2, and PL_1^B) appear as stable phases in the phase diagram, and occupy significant phase regions. The stability of PL phases is not only dependent on the volume fraction but also is strongly dependent on the film thickness. Besides the phase region of the bulk gyroid, the PL phase regions can expand into the lamella and cylinder phase regions by tuning the film thickness. For example, when the film thickness is between $2.4R_g$ and $4.4R_g$ and the volume fraction f is between 0.28 and 0.34, a considerable phase region of the bulk cylinder has been occupied by the PL_1 phase. When the film thickness is increased to form double-layer morphologies, the expansion of the PL_2 phase toward the cylinder or the lamella phase is suppressed. This suggests that the confinement effect tapers as the film thickness is increased, and the phase behaviors tend to approach those in the bulk. This effect can be commonly seen in the comparisons between other types of single-layer and double-layer phases. For example, the invasion of the C_2 phase into S_2 is less than that of the C_1 phase into S_1. Provided that the bulk gyroid phase is replaced by the PL phases, the second feature is that the phase behaviors in a few areas of the phase diagram still resemble the phase sequence in bulk, such as in the area of $2.4R_g < w < 4.4R_g$ and $f < 0.5$ and in the area of $6R_g < w < 8R_g$ and the whole range of f.

To gain quantitative knowledge over the dependence of the OOTs on the film thickness, we plot the free-energy comparison

dx.doi.org/10.1021/jp309546q | J. Phys. Chem. B 2013, 117, 5280−5288

for a given $f = 0.23$ in Figure 3. The bulk phase of this DBC is sphere. Figure 3a indicates that the stable phase transfers from

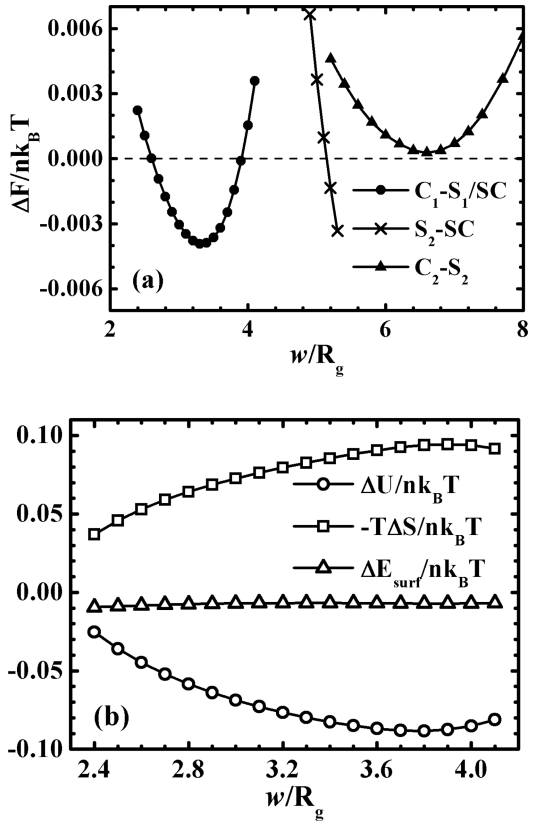

Figure 3. (a) Free-energy difference between two morphologies as a function of film thickness, w/R_g, for a fixed volume fraction of $f = 0.23$. From left to right, the three curves indicate the free-energy difference between the neighbor morphologies of C_1 and S_1 (or SC), S_2 and SC, and C_2 and S_2, respectively. The stable phase sequence is S_1, C_1, SC, and S_2 as the film thickness increases from $2R_g$ to $8R_g$. (b) Three contributions of the free-energy difference between C_1 and S_1: the interfacial energy $\Delta U/nk_BT$, the entropic energy $-T\Delta S/nk_BT$, and the surface interaction $\Delta E_{surf}/nk_BT$.

hexagonally arranged spheres S_1, to parallel cylinders C_1, to elongated spheres SC, and then to double-layer spheres S_2. At this volume fraction, the nonbulk phase of C_1 instead of the bulk phase of S_1 occupies a considerable stable region of $2.6\ R_g < w < 3.9\ R_g$, while the stable phase region of C_2 just vanishes at the phase area of double-layer phases. This phase sequence from sphere, to cylinder, and then to sphere was previously observed by Sevink and Zvelindovsky.[42] In Figure 11 of ref 42, the phase diagram resembles the similar phase sequence in the range of surface field $4.0 < \varepsilon_M < 5.0$. The mechanism of the OOT between S_1 and C_1 can be clarified by the comparisons of three contributions of the free energy in Figure 3b, which are the interfacial energy of $U/nk_BT = (1/V)\int d\mathbf{r}\chi N\phi_A(\mathbf{r})\phi_B(\mathbf{r})$, the entropic energy of $-TS/nk_BT = -\ln Q - (1/V)\int d\mathbf{r}[w_A(\mathbf{r})\phi_A(\mathbf{r}) + w_B(\mathbf{r})\phi_B(\mathbf{r})]$, and the surface interaction of $E_{surf}/nk_BT = (1/V)\int d\mathbf{r}H(\mathbf{r})[\phi_A(\mathbf{r}) - \phi_B(\mathbf{r})]$, respectively. The comparisons demonstrate that the dependence of the interfacial energy and the entropic energy is strong, and that of the surface interaction is moderate. The B-preferential surfaces attract B blocks to form high-density B-block wetting layers, which favors a smaller A/B interface and a smaller mean curvature. This effect can be amplified by simply strengthening the surface interaction. For example, a series of phase transitions from sphere, to cylinder, to perforated lamella, and then to complete lamella has been demonstrated by strengthening the surface field for the sphere-formation DBCs in a thin film with a fixed film thickness of around $4.0R_g$.[42] However, the A/B interface is also influenced by the film thickness. The layer distance in the bulk, $d^*_{hex} = (3)^{1/2}/2d_{hex} \approx 3.28R_g$ of the hex phase, $d^*_{bcc} = (2/3)^{1/2}d_{bcc} = 3.22R_g$ of the bcc phase, and $d^*_{hcp} = (2/3)^{1/2}d_{hcp} = 3.32R_g$ are also readily determined during the free-energy minimization. Whatever morphologies, the favored layer distances are very close. When the film thickness is much smaller than the suitable sphere-layer distance in the bulk, $d^*_{bcc} = (2/3)^{1/2}d_{bcc} = 3.22R_g$, where d_{bcc} is the corresponding domain spacing, the A domains are compressed in the z direction. The compression induces the phase with larger A/B interface to be favored. Therefore, for $w < 2.6R_g < d^*_{bcc}$, the bulk phase of S_1 is stable. When the film thickness is comparable to the bulk layer distance, the cylinder phase C_1 with smaller A/B interface becomes more favorable instead of S_1. While the film thickness becomes larger than d^*_{bcc}, like $w > 3.9R_g$, the A domains have to be elongated to accommodate to the systematical stretching. The corresponding morphologies of S_1 and C_1 are deformed to be SC and $L_{\parallel,\perp}$. Then, the central portion of A domains in SC or $L_{\parallel,\perp}$ becomes cylinder or lamella in a sense. Obviously, the lamellar A domain is extremely unfavorable from the view of chain stretching because the bulk phase is sphere. As the film thickness increases, the unfavorable stretching energy from the central portion of $L_{\parallel,\perp}$ (C_1) becomes more and more dominant, and as a consequence, the phase transfers to SC (S_1). This feature is generic for the other two types of neighbor phases: the PL phase and the cylinder phase (the former one has a smaller mean curvature), the lamellar phase and the PL phase, and so on.

In Figure 4, the domain spacing in the nonconfined xy plane with respect to the film thickness is plotted for $f = 0.23$. As a

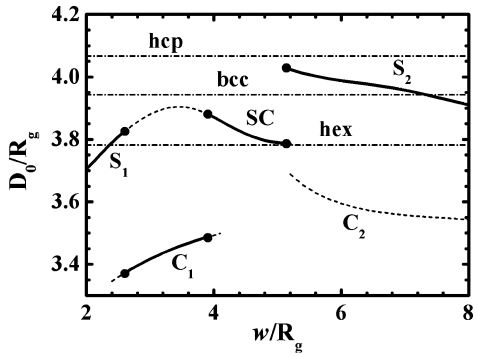

Figure 4. The nearest-neighbor domain spacing in the plane parallel to the surfaces of morphologies S_1 (or SC), C_1, S_2, and C_2 as a function of film thickness, w/R_g, for $f = 0.23$. Solid lines show the spacing variations of stable phase regions, while dashed lines show those of metastable phase regions and dots dividing them indicate the phase transitions. From bottom to top, three dot-dashed lines indicate the nearest-neighbor domain spacing in the bulk phase of hexagonally close-packed (hcp) spheres, body-centered cubic (bcc) spheres, and hexagonally packed cylinders (hex), respectively.

comparison, the corresponding domain spacings of the bulk phases, $d_{hex} \approx 3.78R_g$ of hexagonal cylinders (hex), $d_{bcc} \approx 3.94R_g$ of body-centered-cubic spheres (bcc), and $d_{hcp} \approx 4.07R_g$ of hexagonally close-packed spheres (hcp) are shown by dot-dashed lines. The ratio of the nearest-neighbor sphere-to-sphere distance between the hcp phase and the bcc phase, about 1.03, is

dx.doi.org/10.1021/jp309546q | J. Phys. Chem. B 2013, 117, 5280−5288

consistent with the theoretical value of $(32/27)^{1/6}$.[62] For the hcp phase, we have examined the *abab*··· and *abcabc*··· layer stacking and found that the former stacking is slightly favored. To check the subtle difference of free energy, we repeat the calculations with a finer discretization of Δs = 0.001. The free-energy difference, $(f_{\mathrm{hcp},abc} - f_{\mathrm{hcp},ab})/nk_BT$, is 4.86×10^{-5} and 4.87×10^{-5} for $\Delta s = 0.01$ and $\Delta s = 0.001$, respectively, while that between the hcp (ab) phase and the bcc phase is 3.734×10^{-4} and 3.737×10^{-4}, respectively. At the same time, the discrepancy of the domain spacing computed by the two values of Δs is also negligible small. For example, the sphere-to-sphere distance of the bcc phase for the two cases is $3.943R_g$ and $3.944R_g$, respectively. The tiny discrepancy of the free-energy difference between $\Delta s = 0.01$ and $\Delta s = 0.001$ illustrates that our calculations with $\Delta s = 0.01$ are rather reliable for the determination of phase transitions.

The domain spacing of S_1 for $w < 3.5R_g$ and that of C_1 increase as the film thickness increases, but both are smaller than their bulk values. Larger film thickness induces stronger chain stretching and increases the number of chains contained in each domain, and therefore raises the domain spacing. When the film thickness becomes larger than the bulk layer distance so that it causes the elongation of spheres to form perpendicular cylinders which exhibit smaller domain spacing, the domain spacing tends to drop down. However, in the double-layer morphologies (S_2 and C_2), the situation is inverse. The reason is that the domains in each layer tend to be approaching to reduce the large distance to those in another layer for increasing film thickness.

In Figure 5, we present the plots of free-energy comparisons and corresponding domain spacing as a function of the film thickness for another volume fraction of $f = 0.33$, with which the bulk phase is cylinder, but near the OOT boundary between the cylinder and gyroid phases. The stable phase sequence is from $C_\perp$, to C_1, to PL_1, to C_1 or $L_{\|,\perp}$, to C_2, and then to PL_2. It has been proposed that the stability of PL phases is strongly dependent on the space lattice.[48] In order to clarify this question in our calculations, we performed the calculations with different discretization parameters near an example point of the OOTs, the PL_1–$L_{\|,\perp}$ transition, which is between the film thicknesses of $w = 4.5R_g$ and $w = 4.6R_g$. In the inset of Figure 5a, the free-energy differences between PL_1 and $L_{\|,\perp}$ obtained with four groups of discretization parameters are shown, which are $N_x \times N_y \times N_z = 64^3$ and $\Delta s = 0.01$ (triangles), $N_x \times N_y \times N_z = 128 \times 128 \times 64$ and $\Delta s = 0.01$ (crosses), $N_x \times N_y \times N_z = 64 \times 64 \times 64$ and $\Delta s = 0.002$ (pluses), and $N_x \times N_y \times N_z = 128^3$ and $\Delta s = 0.01$ (circles), respectively. The symbols in the former three cases are almost overlapped, and there is the largest discrepancy in the last case, which is caused only by the increasing of the grid number along the confined direction, N_z. The reason is that the surface potential in the discrete space is dependent on N_z because a short-range potential is employed in our model. However, the discrepancy of the OOT with respect to the film thickness is only as tiny as $0.016R_g$, which is much smaller than the grid spacing, about $0.073R_g$ for $L_z = 4.5R_g$. This clarification further makes sure that our phase diagram is reliable. In fact, PL phases have been observed with cylinder-forming DBCs or ABA triblock copolymers in thin films by a serious of dynamic simulations.[28,40−42,45−47,49] In particular, Ly and co-workers observed a PL phase in a DBC thin film with a similar volume fraction of $f = 1/3$, $\chi N = 18$, and also similar film thickness by using SCFT calculations.[49] Therefore, the prediction by Heckmann and Barbara[48] that the PL phase is unstable is incorrect. In addition,

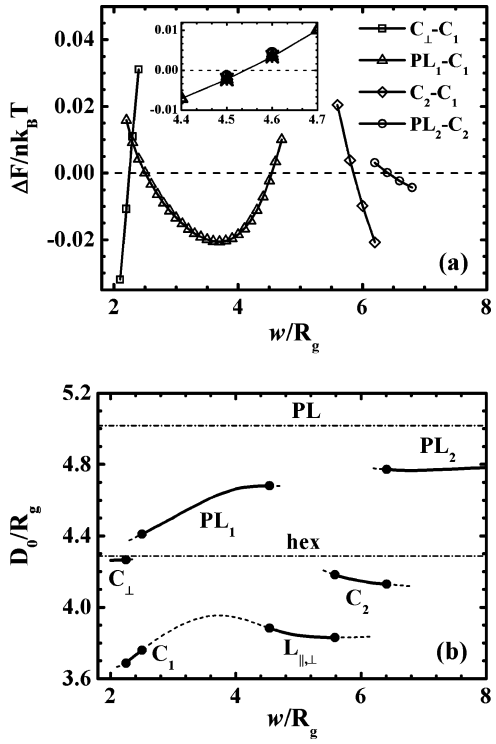

Figure 5. (a) Plot analogue to Figure 3a showing the free-energy differences between neighbor morphologies for $f = 0.33$. The inset shows the free-energy differences between the morphologies of PL_1 and C_1 obtained by different groups of discretization parameters, the lattice size of $N_x \times N_y \times N_z$ and the contour grid spacing of Δs, $N_x \times N_y \times N_z = 64^3$ and $\Delta s = 0.01$ (triangles), $N_x \times N_y \times N_z = 128 \times 128 \times 64$ and $\Delta s = 0.01$ (crosses), $N_x \times N_y \times N_z = 128^3$ and $\Delta s = 0.01$ (circles), and $N_x \times N_y \times N_z = 64^3$ and $\Delta s = 0.002$ (pluses). (b) Plot analogue to Figure 4 showing the nearest-neighbor domain spacing in the plane parallel to the surfaces, of different morphologies for $f = 0.33$. The two dot-dashed lines indicate the nearest-neighbor domain spacing in the bulk of hexagonally packed cylinders and perforated lamellae, respectively.

Kramer et al.[51] have proposed that the magnitude of free-energy difference of the order of 10^{-3} k_BT per chain is sufficient to drive morphological transitions. In Figure 5a, the largest free-energy difference between the PL_1 and C_1 reaches as large as 0.02 k_BT. This indicates that the PL phase can be observed experimentally with a rather wide range of film thickness. From Figure 5b, we can see that the properties of the domain spacings for parallel cylinder phases are quite similar to those in Figure 4. The cylinder-to-cylinder distance of the perpendicular cylinder $C_\perp$ in very thin films is closer to the bulk value than those of these parallel cylinder phases. To have a reference, we have also computed the periods of the metastable PL phase in the bulk. For the bulk PL phase, two feature sizes are required to characterize its periodicity, the nearest-neighbor hole-to-hole distance, d_{PL}, and the distance between two neighbor perforated lamellae, l_{PL}. Similar to the hcp phase, there are two nearly degenerate phases with the *abab*··· and *abcabc*··· stacking of the hexagonally arranged holes, respectively.[62] We first examined the relative stability between *abab*··· with *abcabc*··· PL phases at $f = 0.36$ in the gyroid phase region with $N_x \times N_y \times N_z = 64^3$ and $\Delta s = 0.01$. Our calculations exhibit that the *abcabc*··· PL phase is more favored than the *abab*··· one with a free-energy difference per chain of about 3.433×10^{-4} k_BT for $f = 0.36$, and has lower free energy than both the lamellar phase and the cylinder phase but has higher free energy than the gyroid phase. This prediction is

dx.doi.org/10.1021/jp309546q | J. Phys. Chem. B 2013, 117, 5280−5288

consistent with that in ref 62. Then, we determined the periods of the PL phase at $f = 0.33$, $d_{PL} \approx 5.02R_g$, and $l_{PL} \approx 3.77R_g$. Notably, the PL_1 phase is almost centered around l_{PL} and the hole-to-hole distances of both PL_1 and PL_2 are smaller than the bulk value of d_{PL}. Furthermore, the hole-to-hole distance of PL_2 changes very gently, and is only around 5% smaller than d_{PL}.

When $f > 0.5$, the surfaces attract the minority block B, whose isosurface of density is plotted in green color (see Figure 1). In this case, a central layer of B domains besides the two wetting layers can be formed only when the film is thick enough for the packing of four-layer polymer chains. For example, at $f = 0.7$, the spherical phase S_1^B (denoted as $L_{\parallel} - S_1^B - L_{\parallel}$ in ref 43) becomes stable instead of the lamellar phase $L_1^{\parallel}$ when $w > 1.46d_{hex}^*$, where $d_{hex}^* \approx 3.59R_g$ for $f = 0.7$. At $w > 1.58d_{hex}^*$, the S_1^B phase transfers to the cylindrical phase C_1^B with smaller A/B interface or mean curvature. The mechanism of the OOTs in this phase region is quite similar to that in those single-layer morphologies of $f < 0.5$. When the film is so thin that the polymer chains in the single-layer lamella $L_1^{\parallel}$ are compressed, some half-domain morphologies are formed. For $f = 0.7$, the morphology of double-layer B half-cylinders hC_2^B and that of single-layer B half-lamella $hL_1^{\parallel}$ become stable in sequence when $w < 1.74d_{hex}^*$. The above two phases occupy detectable phase regions in the bottom-right corner of the phase diagram in Figure 2. It is found that the OOT between hC_2^B and $hL_1^{\parallel}$ changes continuously from the first-order transition to the second-order transition (indicated by a dashed line) when $f = 0.75$ is decreased to $f = 0.6$. For example, the first-order transition is observed at $f = 0.72$, while it is hard to be identified at $f = 0.70$. In Figure 6, the free-energy difference between hC_2^B and $hL_1^{\parallel}$ as a function of the film thickness is plotted for $f = 0.68$. It shows that the free energy of hC_2^B is very close to that of $hL_1^{\parallel}$ for $w = 2.163R_g$, but the inset indicates that the former phase still has a slightly higher free energy than the latter. However, at this film thickness, the period of hC_2^B has reached as large as $11.05R_g$. In addition, the period plot with respect to the film thickness suggests that it will go up quickly to be infinite when approaching the transition point, and thus, the hC_2^B phase continuously transforms to $hL_1^{\parallel}$ which is homogeneous in the unconfined space.

In the recent work by Yu et al.,[45] a few cross-cylindrical morphologies, which are composed of two-layer mis-oriented parallel cylinders, have been reported by MC simulations in a range of film thickness of $2.1d_{hex}^* < w < 2.6d_{hex}^*$ with the cylinder-forming DBC of $f = 1/6$. In this range of film thickness, there are two candidate parallel cylindrical morphologies, i.e., the double- and triple-layer cylinders (C_2 and C_3). For the cross-cylindrical morphologies, an interesting characteristic is the angle formed by two mis-oriented cylinders, which seems to be dependent on the film thickness.[45] In computer simulations with a fixed simulation box, the mis-orientation associated with the periodic boundary conditions of the simulation box is an effective way to release the chain stretching energy induced by the mismatch between the domain spacing and the box size. To discern the stability of these cross-cylindrical morphologies, we first build a specific double-layer morphology (denoted as $C_2^{\times}$) from two-layer cylinders with orientations normal to each other and coherent to the side directions of the box, and then compare its free energy with those of its competing morphologies of C_2 and C_3. In the $C_2^{\times}$ morphology, the domain spacings of the two layers are dissociated, and they are the same for the case of identical surfaces. In Figure 7, the density plots of C_3 and $C_2^{\times}$ are shown in parts a and b, and their free-energy comparisons are given in part c, for typical cylinder-forming DBCs with $f = 0.3$. Figure 7c

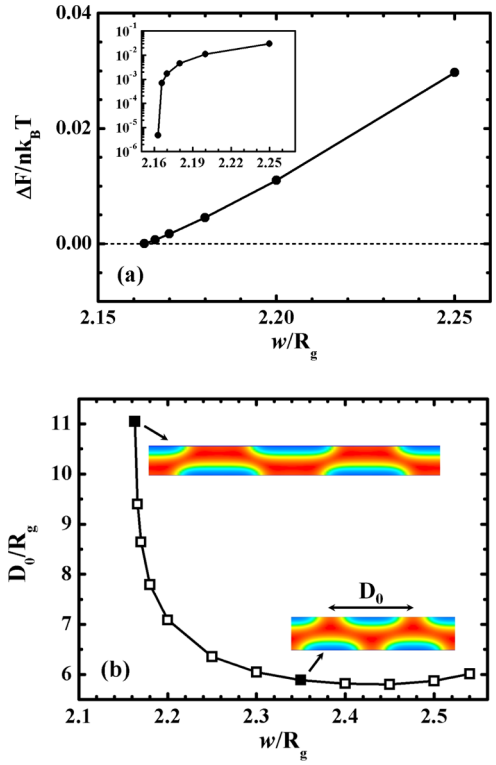

Figure 6. (a) Free-energy difference between the phases hC_2^B and $hL_1^{\parallel}$ as a function of the film thickness for a given $f = 0.68$. The inset gives the corresponding linear-logarithm plot. (b) Period in the unconfined directions, and two typical density profiles of the cross section normal to the domain-aligning direction, at $w = 2.35R_g$ and $w = 2.163R_g$ (two filled symbols), for the phase hC_2^B. The red and blue regions indicate where the dominant components are A and B, respectively.

indicates that the cross-cylindrical morphology $C_2^{\times}$ has consistent higher free energy than C_2 before C_2 transfers to C_3 at $w \approx 2.51d_{hex}^*$. Note that the free-energy difference between $C_2^{\times}$ and C_2 in the range of $2.2d_{hex}^* < w < 2.6d_{hex}^*$ is at least $4 \times 10^{-3}\ k_BT$ per chain, which is hard to be compensated only by regulating the orientations of the cross cylinders. Therefore, we can conclude that the $C_2^{\times}$ morphologies should be metastable.

Our phase diagram with respect to the volume fraction and the film thickness, which has provided a comprehensive picture over the dependence of the OOTs of each composition on the film thickness, can also encompass many of the results in previous studies on thin film systems with two identical strong-preferential surfaces. Next, we will give some direct comparisons between our results and some of the other theoretical work in the literature. Much of the literature reports PL phases in similar film systems with the cylinder-forming DBCs in the similar stable phase regions. Using DDFT simulations, Huinink et al.[40,41] observed the PL_1 phase with $f = 1/3$ and $w \approx 4R_g$ (the original length unit is the grid point; see Figure 6f in ref 40), which is covered by the range $2.47R_g < w < 4.59R_g$ in our phase diagram; they observed PL_1^B with $f = 2/3$ (the surfaces attract the minority block) and PL_2 with $f = 1/3$ for $w \approx 6.86R_g$ (in Figure 5 of ref 41), respectively, which are also almost located in our phase regions of $6.34R_g < w < 8R_g$ (the situation of $w > 8R_g$ is not examined in our phase diagram) and $6.87R_g < w < 8R_g$. With a similar DBC, Ly et al. confirmed the observation of the PL_1 phase with a film thickness of around the bulk cylinder-to-cylinder distance using the dynamic SCFT simulation.[49] In a subsequent work,[42] Sevink and Zvelindovsky systematically studied sphere-forming diblock

dx.doi.org/10.1021/jp309546q | J. Phys. Chem. B 2013, 117, 5280−5288

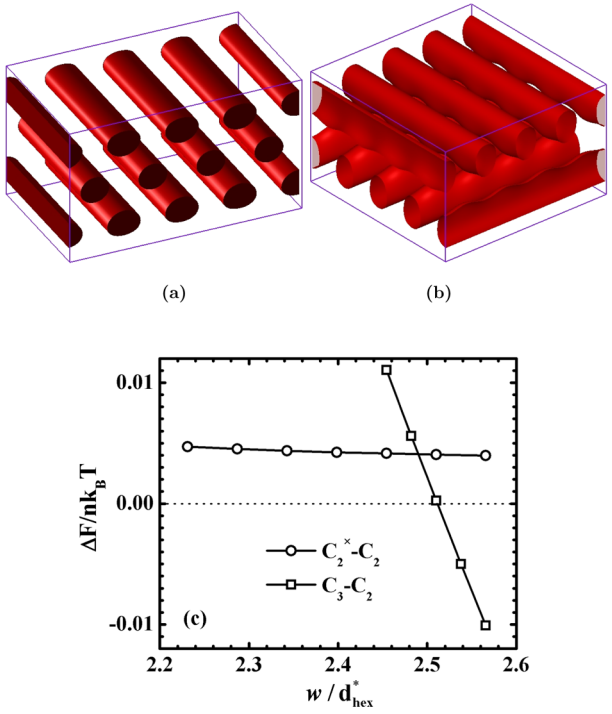

Figure 7. Density isosurface plots of the three-layer cylinders C_3 (a) and the two-layer cross cylinders $C_2^{\times}$ (b) for $f = 0.3$. Part c shows the free-energy comparisons between the three morphologies of C_2, C_3, and $C_2^{\times}$ as a function of the film thickness w in units of d^*_{hex}, which is the neighbor-layer distance of cylinders in the bulk for $f = 0.3$.

copolymers in thin film with a wide range of film thicknesses and surface interactions. They also observed PL morphologies with a number of film thicknesses but with a stronger surface field. Furthermore, with a comparable surface field, $\varepsilon_M \approx 4$, the phase sequence of $S_1 \rightarrow C_\perp \rightarrow S_2$ with $f = 1/3$ and about $3.4R_g \lesssim w \lesssim 8R_g$ in Figure 11 of ref 42 is similar as our $S_1 \rightarrow SC \rightarrow S_2$ with $f = 0.23$ in Figure 2. In Figure 9 of ref 43, Wang et al. observed a similar phase sequence as ours, from $L_1^{\parallel}$, to S_1^B, to PL_1^B, and to C_1^B with $f = 1/4$ using MC simulations except that the sequence between PL_1^B and C_1^B is reversed. In more recent work,[28,45] Li and co-workers have observed the PL morphologies as well as other morphologies in our phase regions. Particularly, their phase sequence with respect to the film thickness for the gyroid-forming DBC of $f = 1/3$ in Figure 5 of ref 28 is consistent with that of $f = 1/3$ in our phase diagram. Besides the results of computer simulations, our results are well consistent with those of available SCFT calculations[46−48] but provide a more detailed phase diagram with respect to the volume fraction and the film thickness. Specifically, Mishra et al.[51] have extensively studied the relative stability between the spherical and cylindrical morphologies as a function of film thickness at the bulk order−order transition temperature, and their results revealed that the cylindrical morphology has a lower free energy at the respective equilibrium film thickness for one-/two-/three-layer structures but with decreasing free-energy difference as the layer number increases. This is consistent with the phase region between $f = 0.23$ and $f = 0.24$ in our phase diagram. A similar mechanism was also exhibited using DDFT simulations by Tan et al.[44]

IV. CONCLUSIONS

We have systematically studied the self-assembly of diblock copolymers confined in two identical surfaces with preferential interactions using the SCFT calculations. A detailed phase diagram with respect to the volume fraction and the film thickness, consisting of more than 200 order−order transition points, has been constructed by considering around 20 candidate morphologies. On the one hand, the phase diagram reveals the impact of the film thickness on the formation of morphologies for each composition going through the entire phase sequence from sphere, to cylinder, to gyroid, and then to lamella. In general, the morphologies with a smaller mean curvature than that of the relevant bulk phase prefer to be formed at the respective commensurate film thickness, particularly for one- and two-layer structures. For example, C_1 is stable instead of S_1 between $2.6R_g < w < 3.9R_g$ at $f = 0.23$; PL_1 is stable instead of C_1 in the region of $2.5R_g < w < 4.5R_g$ at $f = 0.33$. This prediction is consistent with that from the literature by Sevink and co-workers.[42,50,56] On the other hand, the phase diagram explicitly exhibits the shift of order−order transitions induced by the film confinement under the guide of the bulk order−order transitions. In conclusion, our phase diagram provides a comprehensive picture on the complex self-assembling behaviors of diblock copolymers under the confinement of thin film.

AUTHOR INFORMATION

Corresponding Author

*E-mail: weihuali@fudan.edu.cn (W.L.); shi@mcmaster.ca (A.-C.S.).

Notes

The authors declare no competing financial interest.

ACKNOWLEDGMENTS

This work is supported by the National Natural Science Foundation of China (grants 21174031 and 20974026), the National High Technology Research and Development Program of China (863 Grant No. 2008AA032101), the National Basic Research Program of China (2011CB605702), and the Natural Science and Engineering Research Council (NSERC) of Canada.

REFERENCES

(1) Park, M.; Harrison, C.; Chaikin, P. M.; Register, R. A.; Adamson, D. H. *Science* **1997**, *276*, 1401.
(2) Stoykovich, M. P.; Müller, M.; Kim, S. O.; Solak, H. H.; Edwards, E. W.; de Pablo, J. J.; Nealey, P. F. *Science* **2005**, *308*, 1442.
(3) Cheng, J. Y.; Rettner, C. T.; Sanders, D. P.; Kim, H. C.; Hinsberg, W. D. *Adv. Mater.* **2008**, *20*, 3155.
(4) Ruiz, R.; Kang, H.; Detcheverry, F. A.; Dobisz, E.; Kercher, D. S.; Albrecht, T. R.; de Pablo, J. J.; Nealey, P. F. *Science* **2008**, *321*, 936.
(5) Bita, I.; Yang, J.; Jung, Y. S.; Ross, C. A.; Thomas, E. L.; Berggren, K. K. *Science* **2008**, *321*, 939.
(6) Tada, Y.; Akasaka, S.; Yoshida, H.; Hasegawa, H.; Dobisz, E.; Kercher, D.; Takenaka, M. *Macromolecules* **2008**, *41*, 9267.
(7) ITRS International Technology Roadmap for Semiconductors. 2010 Edition. Lithography (http://www.itrs.net/Links/2010ITRS/Home2010.html).
(8) Yang, K. W.; Jung, Y. S.; Chang, J. B.; Mickiewicz, R. A; Alexander-Katz, A.; Ross, C. A.; Berggren, K. K. *Nat. Nanotechnol.* **2010**, *5*, 256.
(9) Huang, E.; Russell, T. P.; Harrison, C.; Chaikin, P. M.; Register, R. A.; Hawker, C. J.; Mays, J. *Macromolecules* **1998**, *31*, 7641.
(10) Huang, E.; Rockford, L.; Russell, T. P.; Hawker, C. J. *Nature* **1998**, *395*, 757.
(11) Busch, P.; Posselt, D.; Smilgies, D.-M.; Rheinlander, B.; Kremer, F.; Papadakis, C. M. *Macromolecules* **2003**, *36*, 8717.
(12) Lambooy, P.; Russell, T. P.; Kellogg, G. J.; Mayers, A. M.; Gallagher, P. D.; Satija, S. K. *Phys. Rev. Lett.* **1994**, *72*, 1994.
(13) Koneripalli, N.; Singh, Nl; Levicky, R.; Bates, F. S.; Gallagher, P. D.; Satija, S. K. *Macromolecules* **1995**, *28*, 2897.

(14) Pickett, G. T.; Balazs, A. C. *Macromolecules* **1997**, *30*, 3097.
(15) Sommer, J. U.; Hoffmann, A.; Blumen, A. *J. Chem. Phys.* **1999**, *111*, 3728.
(16) Geisinger, T.; Müller, M.; Binder, K. *J. Chem. Phys.* **1999**, *111*, 5241.
(17) Tang, W. H. *Macromolecules* **2000**, *33*, 1370.
(18) Tsori, Y.; Andelman, D. *Eur. Phys. J. E* **2001**, *5*, 605.
(19) Frischknecht, A. L.; Curro, J. G.; Douglas Frink, J. *J. Chem. Phys.* **2002**, *117*, 10398.
(20) Shull, K. R. *Macromolecules* **1992**, *25*, 2122.
(21) Turner, M. S. *Phys. Rev. Lett.* **1992**, *69*, 1788.
(22) Walton, D. G.; Kellogg, G. J.; Mayers, A. M.; Lambooy, P.; Russell, T. P. *Macromolecules* **1994**, *27*, 6225.
(23) Kikuchi, M.; Binder, K. *J. Chem. Phys.* **1994**, *101*, 3367.
(24) Matsen, M. W. *J. Chem. Phys.* **1997**, *106*, 7781.
(25) Wang, Q.; Yan, Q.; Nealey, P. F.; de Pablo, J. J. *J. Chem. Phys.* **2000**, *112*, 450.
(26) He, X.; Song, M.; Liang, H.; Pan, C. *J. Chem. Phys.* **2001**, *114*, 10510.
(27) Feng, J.; Liu, H.; Hu, Y. *Macromol. Theory Simul.* **2002**, *11*, 549.
(28) Yin, Y.; Sun, P.; Jiang, R.; Li, B.; Chen, T.; Jin, Q.; Ding, D.; Shi, A.-C. *J. Chem. Phys.* **2006**, *124*, 184708.
(29) Meng, D.; Wang, Q. *Soft Matter* **2010**, *6*, 5891.
(30) Liu, Y.; Zhao, W.; Zheng, X.; King, A.; Singh, A.; Rafailovich, M. H.; Sokolov, J.; Dai, K. H.; Kramer, E. J.; Schwarz, S. A.; Gebizlioglu, O.; Sinha, S. K. *Macromolecules* **1994**, *27*, 4000.
(31) Henkee, C. S.; Thomas, E. L.; Fetters, J. J. *J. Mater. Sci.* **1988**, *23*, 1685.
(32) Karim, A.; Singh, N.; Sikka, M.; Bates, F. S.; Dozier, W. D.; Felcher, G. P. *J. Chem. Phys.* **1994**, *100*, 1620.
(33) Mansky, P.; Chaikin, P.; Thomas, E. L. *J. Mater. Sci.* **1995**, *30*, 1987.
(34) Radzilowski, L. H.; Carvalho, B. L.; Thomas, E. L. *J. Polym. Sci., Part B: Polym. Phys.* **1996**, *34*, 3081.
(35) Park, M.; Harrison, C.; Chaikin, P. M.; Register, R. A.; Adamson, D. H.; Yao, N. *Mater. Res. Soc. Symp. Proc.* **1997**, *461*, 179.
(36) Harrison, C.; Park, M.; Chaikin, P. M.; Register, R. A.; Adamson, D. H.; Yao, N. *Polymer* **1998**, *39*, 2733.
(37) Harrison, C.; Park, M.; Chaikin, P. M.; Register, R. A.; Adamson, D. H.; Yao, N. *Macromolecules* **1998**, *31*, 2185.
(38) Smith, A. P.; Douglas, J. F.; Meredith, J. C.; Amis, E. J.; Karim, A. *Phys. Rev. Lett.* **2001**, *87*, 015503.
(39) Tsarkova, L.; Knoll, A.; Krausch, G.; Magerle, R. *Macromolecules* **2006**, *39*, 3608.
(40) Huinink, H. P.; Brokken-Zijp, J. C. M.; van Dijk, M. A.; Sevink, G. J. A. *J. Chem. Phys.* **2000**, *112*, 2452.
(41) Huinink, H. P.; van Dijk, M. A.; Brokken-Zijp, J. C. M.; Sevink, G. J. A. *Macromolecules* **2001**, *34*, 5325.
(42) Sevink, G. J. A.; Zvelindovsky, A. V. *Macromolecules* **2009**, *42*, 8500.
(43) Wang, Q.; Nealey, P. F.; de Pablo, J. J. *Macromolecules* **2001**, *34*, 3458.
(44) Tan, H.; Song, Q.; Niu, X.; Wang, Z.; Gao, W.; Yan, D. *J. Chem. Phys.* **2009**, *130*, 214901.
(45) Yu, B.; Li, B.; Jin, Q.; Ding, D.; Shi, A.-C. *Soft Matter* **2011**, *7*, 10227.
(46) Yang, Y.; Qiu, F.; Zhang, H.; Yang, Y. *Polymer* **2006**, *47*, 2205.
(47) Chen, P.; Liang, H. J.; Shi, A.-C. *Macromolecules* **2007**, *40*, 7329.
(48) Heckmann, M.; Drossel, B. *Macromolecules* **2008**, *41*, 7679.
(49) Ly, D. Q.; Honda, T.; Kawakatsu, T.; Zvelindovsky, A. V. *Macromolecules* **2008**, *41*, 4501.
(50) Horvat, A.; Lyakhova, K. S.; Sevink, G. J. A.; Zvelindovsky, A. V.; Magerle, R. *J. Chem. Phys.* **2004**, *120*, 1117.
(51) Mishra, V.; Fredrickson, G. H.; Kramer, E. J. *Macromolecules* **2011**, *44*, 5473.
(52) Szamel, G.; Müller, M. *J. Chem. Phys.* **2003**, *118*, 905.
(53) Stein, G. E.; Cochran, E. W.; Katsov, K.; Fredrickson, G. H.; Kramer, E. J.; Li, X.; Wang, J. *Phys. Rev. Lett.* **2007**, *98*, 158302.
(54) Stein, G. E.; Kramer, E. J.; Li, X.; Wang, J. *Macromolecules* **2007**, *40*, 2453.
(55) Bosse, A. W.; Garcia-Cervera, C. J.; Fredrickson, G. H. *Macromolecules* **2007**, *40*, 9570.
(56) Knoll, A.; Horvat, A.; Lyakhova, K. S.; Krausch, G.; Sevink, G. J. A.; Zvelindovsky, A. V.; Magerle, R. *Phys. Rev. Lett.* **2002**, *89*, 035501.
(57) Shi, A.-C. In *Development in Block Copolymer Science and Technology*; Hamley, I. W., Ed.; Wiley: New York, 2004.
(58) Fredrickson, G. H. *The Equilibrium Theory of Inhomogeneous Polymers*; Oxford University Press: Oxford, U.K., 2006.
(59) Li, W. H.; Wickham, R. A. *Macromolecules* **2009**, *42*, 7530.
(60) Tzeremes, G.; Rasmussen, K. Ø.; Lookman, L.; Saxena, A. *Phys. Rev. E* **2002**, *65*, 041806.
(61) Rasmussen, K. Ø.; Kalosakas, G. J. *J. Polym. Sci., Part B: Polym. Phys.* **2002**, *40*, 1777.
(62) Matsen, M. W.; Bates, F. S. *J. Chem. Phys.* **1997**, *106*, 2436.